Journal of Proteomics 179 (2018) 30–41

Contents lists available at ScienceDirect

Journal of Proteomics

journal homepage: www.elsevier.com/locate/jprot

Longissimus dorsi muscle label-free quantitative proteomic reveals biological mechanisms associated with intramuscular fat deposition

Mirele D. Poleti[a], Luciana C.A. Regitano[b], Gustavo H.M.F. Souza[c], Aline S.M. Cesar[a], Rosineide C. Simas[a,1], Bárbara Silva-Vignato[d], Gabriella B. Oliveira[a,2], Sónia C.S. Andrade[a,3], Luiz C. Cameron[e,f], Luiz L. Coutinho[a,*]

[a] Department of Animal Science, "Luiz de Queiroz" College of Agriculture, University of São Paulo/ESALQ, Piracicaba, SP 13418-900, Brazil
[b] Embrapa Pecuária Sudeste, São Carlos, SP 13560-970, Brazil
[c] MS Applications and Development Laboratory Waters Corporation, São Paulo, SP 06455-020, Brazil
[d] Department of Animal Science, College of Animal Science and Food Engineering, University of São Paulo/FZEA, Pirassununga, SP 13635-900, Brazil
[e] Laboratory of Protein Biochemistry, Federal University of State of Rio de Janeiro/UNIRIO, Rio de Janeiro, RJ 22290-255, Brazil
[f] Department of Biochemistry and Sportomics, Olympic Laboratory, Brazil Olympic Committee, Rio de Janeiro, RJ, Brazil

ARTICLE INFO

Keywords:
Adiposity
Biological processes
Mass spectrometry
microRNA
mRNA
Protein

ABSTRACT

The pathways involved in intramuscular fat (IMF) deposition in *Longissimus dorsi* muscle were investigated using an integrated transcriptome-assisted label-free quantitative proteomic approach by High Definition Mass Spectrometry. We quantified 1582 proteins, of which 164 were differentially abundant proteins (DAPs, $p < 0.05$) between animals with high (H) and low (L) genomic estimated breeding values (GEBV) for IMF content. Ingenuity pathway analysis (IPA) revealed that these DAPs were mainly involved in glycolysis metabolism, actin cytoskeleton signaling, cell-cell adherens junction and pathways for MAPK and insulin. A comparative study between transcriptomic (mRNA) and proteomic data showed 17 differentially expressed genes corresponding to DAPs, of which three genes/proteins did not agree on the direction of the fold change between groups. Moreover, we investigated microRNAs data to explain these differences in fold change direction, being able to unravel two of the three unexpected mRNA/protein relationships. Results demonstrated that changes in protein/mRNA levels of sarcomere organization, intracellular signal transduction and regulation of actin cytoskeleton, are involved in IMF deposition. These findings provide a deeper understanding of the highly complex regulatory mechanisms involved in IMF deposition in cattle and indicate target pathways for future studies.

Significance: Intramuscular fat is the amount of fat deposited inside muscle and plays an important role in human health and meat quality attributes, influencing energy metabolism of skeletal muscle, as well as, tenderness, flavor, and juiciness of beef. We performed for the first time the utilization of integrated transcriptome-assisted label-free quantitative proteomic approach using High Definition Mass Spectrometry for characterization of the changes in the proteomic profile of the *Longissimus dorsi* muscle associated with intramuscular fat deposition in cattle. Furthermore, we compared the muscle proteome with the muscle transcriptome (mRNA and microRNAs), obtained by RNA-sequencing, to better understand the relationship between expression of mRNAs and proteins and to unravel essential biological mechanisms involved in bovine skeletal muscle IMF deposition.

1. Introduction

The amount of lipid accumulation between muscle fiber bundles is of particular importance to human health and the beef industry since it contributes to beef quality, nutritional content, and carcass value. Intramuscular fat (IMF), also known as marbling, impacts energy metabolism and insulin signaling in skeletal muscle [1], as well as tenderness, juiciness, flavor and shelf life (lipid and pigment oxidation) of beef [2,3].

IMF deposition occurs later in life. As the animal approaches mature weight, there is a decrease in myofiber hypertrophy and an increase in fat deposition. Cellular and molecular networks involved in

* Corresponding author at: "Luiz de Queiroz" College of Agriculture, University of São Paulo, Av. Pádua Dias, 11, 13418-900 Piracicaba, São Paulo, Brazil.
E-mail address: llcoutinho@usp.br (L.L. Coutinho).
[1] Current address: Faculty of Pharmacy of the Federal University of Rio de Janeiro, Rio de Janeiro-RJ, 21941–590, Brazil.
[2] Current address: Federal University of Rio Grande do Sul, Porto Alegre-RS, 90040–060, Brazil.
[3] Current address: Genetics and Evolutionary Biology Department, University of São Paulo, São Paulo-SP, 05508–090, Brazil.

https://doi.org/10.1016/j.jprot.2018.02.028
Received 25 November 2017; Received in revised form 14 February 2018; Accepted 26 February 2018
Available online 03 March 2018
1874-3919/

adipogenesis and myogenesis regulate the dynamic balance between the number and size of adipocytes and myocytes [4]. However, the proportion fat and muscle is highly variable and influenced by genetics, age, sex and nutrition [2,5].

Recent studies evaluating mRNA expression to elucidate molecular processes involved in IMF deposition in skeletal muscle identified hundreds of genes involved in several biochemical pathways and cellular signaling mechanisms [6–8]. However, mRNA expression levels are not highly correlated with protein abundance [9,10]. Hence, proteomics has emerged as an important investigation tool to complement genomic studies and provide a deeper understanding of complex biological processes.

Recent proteomic studies addressed differences in IMF deposition between individuals from different breeds [11,12], between breeds [13], and in distinct stages of IMF development [14,15]. Nevertheless, genetic mechanisms involved in IMF deposition are not completely clear.

Proteomic analysis based on two-dimensional electrophoresis and mass spectrometry has been used successfully to study skeletal muscle [16–19], but recent technological innovations in liquid chromatography, mass spectrometry, and bioinformatics have allowed more concise and complex results in proteomics [20,21]. Label-free quantitative proteomics by High Definition Mass Spectrometry (HDMS^E) has become an attractive and powerful analytical tool to analyze the abundance of thousands of proteins in complex biological samples due to its high technical reproducibility, improved proteome coverage, as well as more confident peptide identification and quantification [22,23].

In the present study, we investigated the differences on protein profile of *Longissimus dorsi* muscle samples of animals with High (H) and Low (L) genomic estimated breeding values for IMF content using an integrated transcriptome-assisted label-free quantitative proteomic approach by High Definition Mass Spectrometry (HDMS^E). Moreover, we compared proteomic results with transcriptomic results of mRNAs and microRNAs from the same animals [6,24], to better explore and clarify the biological mechanisms that influence IMF deposition.

2. Materials and methods

2.1. Animals and samples

A population of 390 male Nelore animals, progenies of 34 unrelated sires representative of the main Nelore genealogies used in Brazil, were used in this experiment. The animals were raised on pasture until approximately 21 months of age when they were allocated to feedlots. The same diet and handling conditions were provided to all animals. The animals were slaughtered at an average live weight of 452 ± 50 kg and 24 ± 1 month of age. All procedures related to animal experiments were undertaken following the Institutional Animal Care and Use Committee Guidelines (IACUC) from Brazilian Agriculture Research Corporation (EMBRAPA) and approved by the director Dr. Rui Machado.

Samples were excised from *Longissimus dorsi* (LD) muscle located between 12th and 13th ribs. For proteomics analysis, samples were collected immediately after slaughter, snap frozen in liquid nitrogen and stored at −80 °C. For measurement of the intramuscular fat (IMF) content, samples was collected 24 h after slaughter, vacuum packaged and stored at −20 °C.

The IMF content (%), backfat thickness (BFT, mm) and ribeye area (REA, cm^2) data used herein were previously reported [6,25]. From this data set, 20 samples from animals with extreme genomic estimated breeding values (GEBV) for IMF content were selected for this proteomic study. The subject group with higher GEBV values was named High (H, n = 10), and the subject group with lower GEBV values was named Low (L, n = 10). GEBV were computed under the Genomic Best Linear Unbiased Prediction (GBLUP) model using ASREML 3.0 software [26] as previously published [6] for 390 animals. The statistical model included contemporary animal groups with the same origin, birth year and slaughter date as fixed effect, and hot carcass weight as a covariate. The Student's t-test was used to evaluate the differences between the L and H groups for IMF, BFT, and REA by R software.

2.2. Muscle protein extraction

Pieces of frozen muscle were ground under liquid nitrogen, transferred to a microcentrifuge tube and weighed still frozen in order to minimize protein degradation. Approximately 0.5 g of frozen muscle were homogenized in 2.5 mL lysis buffer containing 8 M Urea, 2 M Thiourea, 1% DTT, 2% CHAPS and 1% Protease Inhibitor Cocktails (Sigma-Aldrich) in ULTRA-TURRAX® IKA homogenizer on ice. Extracts were vigorously shaken for 30 min on ice and centrifuged at 10,000 × g for 30 min at 4 °C. The supernatants were collected and total protein concentration determined by PlusOne 2-D Quant Kit (GE Healthcare). Samples were stored at −80 °C until required for further analysis.

2.3. Sample preparation for mass spectrometry

The protein extract was desalted using a 3-kDa cutoff Amicon® Ultra centrifugal filter (Millipore, Ireland), where the lysis buffer was exchanged with a solution of 50 mM ammonium bicarbonate and 2 M urea for five times. The concentration of retained protein solution was quantified using a Bradford Protein Assay Kit (BioRad). For protein digestion, 50 μg of proteins of each sample were denatured with 25 μL of 0.2% *Rapi*Gest SF (Waters Corporation, USA) at 80 °C for 15 min, reduced with 2.5 μL of 100 mM dithiothreitol (DTT) (Sigma, USA) at 60 °C for 30 min, and alkylated with 2.5 μL of 300 mM iodoacetamide (AA) (Sigma, USA) at room temperature in the dark for 30 min. Enzymatic digestion was performed with sequencing grade modified trypsin (Promega) at a 1:100 (w/w) enzyme: protein ratio at 37 °C for 16 h. Digestion was stopped by the addition of 10 μL of 5% (V/V) trifluoroacetic acid, and incubated at 37 °C for 90 min to hydrolyze the *Rapi*Gest [27]. The peptide mixture solution was then centrifuged at 18,000 × g for 30 min at 6 °C. The supernatant was transferred to a new vial, dried down in a vacuum centrifuge and stored at −20 °C.

2.4. nanoUPLC-HDMS^E analysis

Qualitative and quantitative bidimensional nanoUPLC tandem nanoESI-HDMS^E analyses were conducted using both 1 h reversed phase gradient from 7% to 40% (v/v) acetonitrile (0.1% v/v formic acid) and 500 nL·min.$^{-1}$ on a nanoACQUITY UPLC 2D Technology system [28]. A nanoACQUITY UPLC HSS T3 1.8 μm, 75 μm × 15 cm column (pH 3) was used in conjunction with a reverse phase (RP) XBridge BEH130 C18 5 μm 300 μm × 50 mm nanoflow column (pH 10). Typical on-column sample loads were 500 ng of total protein digests for each of the 3 fractions (500 ng/fraction/load). The ion mobility cell was activated and filled with nitrogen gas, which operates at the cross-section resolving power of at least 40 Ω/ΔΩ [29]. The effective resolution with the conjoined ion mobility were > 1.5 M FWHM [30]. Ionization of the samples was performed using a NanoLockSpray ionization source (Waters, Manchester, UK) in the positive ion mode nanoESI (+). Lock mass channel was sampled every 30 s. The mass spectrometer was calibrated with a MS/MS spectrum of [Glu^1]-Fibrinopeptide B human (Glu-Fib) solution (100 fmol·uL^{-1}) delivered through the reference sprayer of the NanoLockSpray source. The $[M + 2H]^{2+}$ = 785.8426 was used for initial single-point calibration and MS/MS fragment ions of Glu-Fib were used to obtain the final instrument calibration. Data acquisition was performed using a Synapt G2-S HDMS mass spectrometer (Waters, Manchester, UK). Data was acquired under multiplexed data-independent (DIA) scanning with added specificity and selectivity of a non-linear 'T-wave' ion mobility (HDMS^E) device. The mass spectrometer was automatically planned to do the following: (a) switch

between standard MS (3 eV) and elevated collision energies HDMS^E (19–45 eV) applied to the transfer 'T-wave' CID (collision-induced dissociation) cell filled with argon gas; (b) adjust the trap collision cell to 1 eV. Scan time was 500 m-seconds, previously adjusted based on the linear flow velocity of the chromatography peak delivered from nano-binary pumps to obtain a minimum of 20 scan points for each individual peak, both in low energy and high-energy transmission on an orthogonal acceleration time-of-flight (*oa*-TOF). A mass range from *m/z* 50 to 2000 was utilized. The radio-frequency (RF) offset (MS profile) was adjusted so that the nanoUPLC-HDMS^E data were effectively acquired from *m/z* 400 to 2000, which ensured that any masses observed in the high energy spectra with less than *m/z* 400 arose from dissociations in transferring the collision cell.

2.5. Data analysis

Mass spectrometry data were acquired with Waters MassLynx v.4.1 software and processed using Progenesis QI for Proteomics (QIP) 2.0 software (Nonlinear Dynamics, UK). Progenesis QIP software was used to run alignment, peak picking, ion drift time data collection, ion abundance measurements, normalization, quantification, peptide & protein identification and statistical analysis. The processing parameters for Progenesis included the following: automatic tolerance for precursor and product ions based on peptide identification and a normal distribution [31], one missed cleavage, carbamidomethylation of cysteine as fixed modification, and oxidation of methionine as variable modification. For protein identification and quantification, the obtained raw data were searched against a Nelore transcriptome database built from RNA-sequencing data from LD muscle. To access the false positive rate of identification, the databases utilized were reversed "on-the fly" during the database queries and appended to the original database. A maximum false discovery rate (FDR) was set to 4% [32–36]. Label-free protein quantification values were generated based on the label-free Hi3 method, as described before [37,38].

Data quality assessment were performed accordingly [39], and proteins were selected based on the detection and identification in at least 8 of 10 biological replicates per group. Differentially abundant proteins (DAP) were considered and filtered by ANOVA test (p-value < 0.05).

The partial correlation coefficients between mRNA/microRNA and protein/microRNA were computed by Partial Correlation with Information Theory (PCIT) analysis [40] using the whole list of proteins abundance data as well as microRNAs and mRNAs expression levels data. The mRNA and microRNA data used in this study were previously published [6,24], respectively.

2.6. Transcriptome database assembly

The LD muscle RNA-Sequencing data [5] from the 20 animals used in this study, plus 23 extra from the same population to insure genetic diversity, were used to build Nelore transcriptome database for this study. All the dataset is available in the in the European Nucleotide Archive (ENA) repository (EMBL-EBI), under accession PRJEB13188 [http://www.ebi.ac.uk/ena/data/view/PRJEB13188]. Seqyclean v1.9 software (https://bitbucket.org/izhbannikov/seqyclean/downloads) was used to filter reads with a minimum Phred base quality of 26, and reads longer than 65 bp (base pairs) in length; furthermore, vector and adaptor sequences were identified by comparing reads to the Univec database (https://www.ncbi.nlm.nih.gov/tools/vecscreen/univec/) to remove possible artificial sequence contaminants. Following this filtering step, around 284 million reads were normalized using the script normalize_by_kmer_coverage.pl from Trinity v2.1.1 [41,42]. A total of 133,384,146 reads obtained from the normalization step was used in the assembly. The reference assembly was performed with Trinity v2.1.1, and only the contigs longer than 300 bp were recovered. Reduction of redundant reads in the assembly was performed with CD-HIT version 4.6 [43] using a threshold of 98% global similarity, followed by identification and removal of low-complexity sequences using DustMasker [44]. The reduced assembly was then processed in TransDecoder [42] to identify candidate ORFs within the transcripts. Assembled data were compared to NCBI's UniProt database with the BLASTX tool with a cutoff of $1\,e^{-5}$. Sequences with hits to rRNA (ribosomal RNA) sequences were excluded.

2.7. Functional enrichment analysis

Functional enrichment analysis was performed using the list of the proteins with significant difference ($p < 0.05$) in abundance between the H and L groups by Biological Network Gene Ontology – BiNGO [45], an app from Cytoscape [46]. The redundant GO terms generated were summarized in clusters by REVIGO tool [47]. Canonical pathways, upstream regulators, and network analysis were performed by Ingenuity Pathway Analysis software (IPA-http://www.ingenuity.com) using inputs of gene identifiers, log2fold-changes between H and L groups. Protein-protein interactions were analyzed by STRING version 10 (http://string-db.org) [48] against *Bos taurus* database and considering a medium confidence score of 0.4 for interactions. Biological processes, cellular components, molecular functions, and KEGG pathways analysis were conducted using DAVID (Database for Annotation, Visualization, and Integrated Discovery) version 6.7 [49]. The DAPs and DEGs lists were first analyzed separately and later combined for a more comprehensive analysis.

3. Results

3.1. Phenotypic data

The intramuscular fat (IMF), backfat thickness and ribeye area for the selected animals are presented in Table 1. More information on the phenotypes and GEBV for each animal are reported in supplementary Table S1 in *Data in Brief* article. Statistically significant differences between H and L groups were observed only for IMF percentage ($p < 0.001$) demonstrating the representative biological relevance of samples selected for this trait. The genetic variance, residual variance, and heritability obtained for IMF content from this population were 0.196; 0.490; 0.29 ± 0.16, respectively [50].

3.2. Proteomic data

To increase the coverage of the overall muscle proteome for differential proteomics analysis between H and L groups, we used multidimensional nanoUPLC combined with a hybrid Ion Mobility Q-Tof mass spectrometer with step-wave ion optics. To enhance peptide detection and confidence of proteins identification, we assembled and used transcriptome data from Nelore LD muscle for proteomics data analysis. The de novo *transcriptome* assembly contained 366,987 contigs, with N50 of 3166 and a mean contig length of 1446.3 bp, after reduction. From this total, 100,277 contigs had hit against the UniProt database, and 113,178 contigs were translated by TransDecoder.

The label-free proteome profile identified 19,922 peptides with an error < 5 ppm, of which 9110 were unique peptides. A total of 2529

Table 1
Mean values [± standard deviation] of intramuscular fat [IMF], backfat thickness and ribeye area for High and Low groups based on genomic estimated breeding values [GEBV] for IMF percentage from *Longissimus dorsi* muscle.

Traits	High IMF		Low IMF		p-value
Intramuscular fat [%]	4.56	± 0.40	1.54	± 0.25	< 0.001
Back fat thickness [mm]	5.00	± 1.75	5.30	± 1.35	0.688
Ribeye area [cm^2]	61.35	± 8.95	58.78	± 7.03	0.362

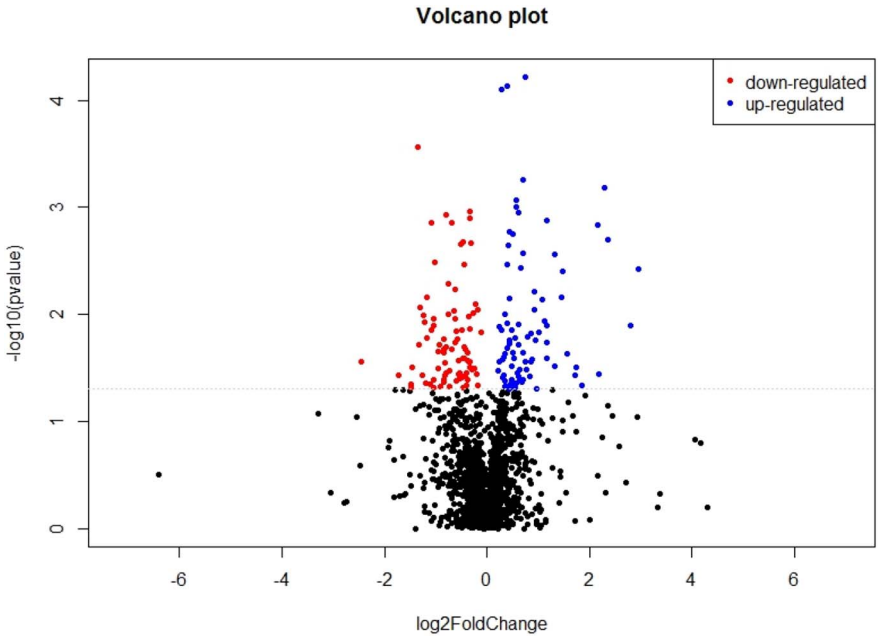

Fig. 1. Volcano plot shows ANOVA p-values [y-axis] plotted against log2 values of protein fold changes [x-axis] for quantitative analysis of proteins abundance comparing High vs. Low groups, classified on genomic estimated breeding values for intramuscular fat. Blue and red dots represent significant [$p < 0.05$] up and down-regulated proteins, respectively. (For interpretation of the references to colour in this figure legend, the reader is referred to the web version of this article.)

proteins were identified with an average of 7 peptides per protein (Supplementary Table S2, *Data in Brief* article). From these, only proteins present in at least eight biological replicates and identified with at least two peptides were used in differential abundance analysis, resulting in 18,100 peptides and 1582 proteins quantified (Supplementary Table S3, *Data in Brief* article). The average coefficient of variation for protein abundance was 0.51 and 0.52 for H and L groups, respectively. Of the 1582 quantified proteins, 164 were differentially abundant proteins (DAPs, $p < 0.05$) between the two groups; 83 proteins were down-regulated and 81 up-regulated in H group (Fig. 1, and Supplementary Table S4 in *Data in Brief* article). The lowest fold change (-2.46) among the DAP was for the Copine-8 protein (CPNE8), and the highest fold change (2.95) was for Protein FAM135A.

3.3. Functional enrichment and pathway analysis of DAPs

To better understand the biological processes in which the DAPs were involved, we performed functional enrichment analysis of the 164 DAPs by Gene Ontology (GO) terms using BiNGO v.3.0.3. Twenty-eight Biological Processes (BP), 50 Molecular Functions (MF) and 16 Cellular Components (CC) were enriched (FDR < 0.1), which were summarized in non-redundant GO terms by REVIGO. REVIGO assigned 20 GO terms to BP, 37 to MF and 14 to CC (Supplementary Table S5, *Data in Brief* article). The most significantly enriched terms for the biological process included monosaccharide catabolism, alcohol catabolism, carbohydrate catabolism, and small molecule catabolism. Enriched molecular function terms predominantly revealed proteins involved in binding, catalytic activity, coenzyme binding, ATP binding, hydrolase activity, purine nucleotide binding, ATPase activity, ion binding, cation binding, and metal ion binding. With respect to the cellular component, we identified proteins mainly related to cytoplasm and intracellular space (Fig. 2).

Core analysis by IPA software identified four significant canonical pathways (determined by Fisher's exact test right-tailed from DAP list, adjusted p-value < 0.05, Table 2). All proteins involved in the glycolysis pathway were down-regulated in the H group (Fig. 3).

IPA upstream regulator analysis was performed to help explain the observed protein abundance changes, which predicted (p-value < 0.10) Insulin 1 (*Ins1*) and Mitogen-activated protein kinase 1 (*MAPK1*) as significant activated upstream regulators (activation z-score 2.236 for both, Fig. 4). The z-scores infer the activation states of predicted transcriptional regulators, being z-score > 2 or < -2 indicative that the activity of a relevant function was significantly increased or decreased.

The top five associated network functions identified from the list of DAP were related to development disorder; cellular assembly and organization; cellular function and maintenance; nucleic acid metabolism, and cell death and survival (Supplementary Table S6, *Data in Brief* article). We found six proteins associated with lipid metabolism within these networks: Pyruvate dehydrogenase (PDK4), Pyruvate dehydrogenase E1 component subunit beta (PDHB), Long-chain-fatty-acid-CoA ligase 1 (ACSL1), Microtubule-associated protein tau (MAPT), Synaptojanin-1 (SYNJ), and Thymidine kinase 2, mitochondrial (TK2).

A network of physical and functional protein-protein interactions (PPI) was built using STRING v. 10.0 online software against *Bos taurus* database. A total of 206 known or predicted interactions (*PPI enrichment* p-value $= 3.53\,e^{-10}$) were formed among DAPs in the PPI network (Fig. 5). The highest number of interactions was observed for Heat shock protein HSP 90-alpha (HSP90AA1). Dense networks associations were also observed around Beta-enolase (ENO3), CAD protein (CAD), Inosine-5′-monophosphate dehydrogenase 2 (IMPDH2), L-lactate dehydrogenase B chain (LDHB) e Alpha-actinin-1 (ACTN1).

KEGG pathway analysis using STRING revealed three significant biochemical pathways: carbon metabolism (bta:01200, FDR $= 3.29\,e^{-05}$), Glycolysis/Gluconeogenesis (bta:00010, FDR $= 0.00101$), and microbial metabolism in diverse environments (bta:01120, FDR $= 0.00255$).

3.4. Comparative analysis of proteomic and transcriptomic data

A comparative study was carried out using our proteomic results and the transcriptome data from a previous study of our group on the same biological samples [6]. In the RNA-seq study, out of 16,101 genes identified in LD muscle, 1129 were differentially expressed genes (DEGs, $p < 0.05$) between H and L groups. In this study, 1582 proteins were quantified and 164 were DAPs. There were 17 genes differentially expressed at the mRNA and protein levels (Table 3).

Transcriptomic and proteomic results were not consistent on the sign of the fold change between H and L groups for three genes/proteins (*DIS3L*, *DPYSL2*, and *LRRFIP1*). Two (*DPYSL2* and *LRRFIP1*) had lower mRNA expression and higher protein abundance in H compared to L group. While *DIS3L* demonstrated higher mRNA expression and lower protein abundance in H compared to L group (Table 3). The results for

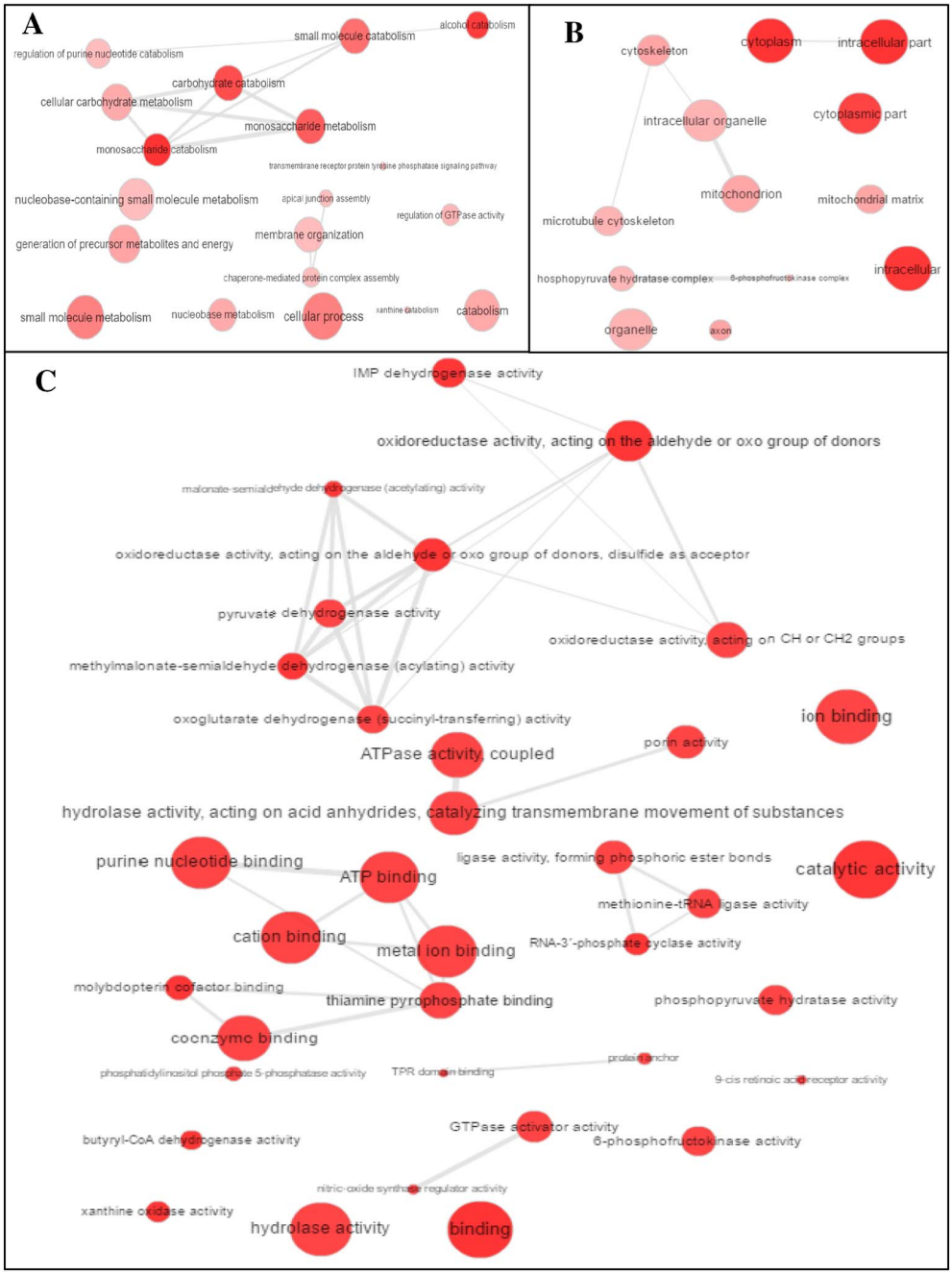

Fig. 2. The interactive graph view from REVIGO for the enriched terms [FDR < 10%] of biological processes [A], cellular component [B] and molecular function [C] for the differentially abundant proteins between High vs. Low groups based on genomic estimated breeding values for intramuscular fat. The bubble colour indicates the p-value and bubble size indicates the frequency of the GO term in the underlying GO database.

Table 2
Significant canonical pathways [adjusted p-value < 0.05] identified by Ingenuity Pathway Analysis [IPA] from the list of differentially abundant proteins.

Ingenuity canonical pathways	B-H p-value[a]	Number of molecules
Glycolysis I	4.92E-03	4
Actin Cytoskeleton Signaling	4.92E-03	9
Remodeling of epithelial adherens junction signaling	1.09E-02	5
Huntington's disease signaling	2.20E-02	8

[a] B-H p-value: p-value corrected for multiple testing by Benjamin-Hochberg False Discovery Rate [FDR] procedure.

DIS3L, DPYSL2, and LRRFIP1 protein abundance could be explained by a higher expression of microRNAs (miRNAs) that targets these genes. Taking this into consideration, we investigated the miRNAs expression from a previous study of our group [24]. Among the differentially expressed miRNAs ($p < 0.05$), eight had as target the DIS3L and higher expression in the H group. Eight had as target the DPYSL and higher expression in the L group. The correlation values were calculated between the expression levels of these miRNAs and the DIS3L and DPYSL2 proteins (Table 4).

A negative correlation was observed between DIS3L protein and the miRNAs bta-mir-339a, bta-mir-339b and bta-mir-423-5p. For the DPYSL2 protein, a negative correlation was found with the miRNAs bta-mir-1388-5p, bta-mir-143, bta-mir-30a-5p, and bta-mir-874. These results could explain the higher mRNA expression level and the lower

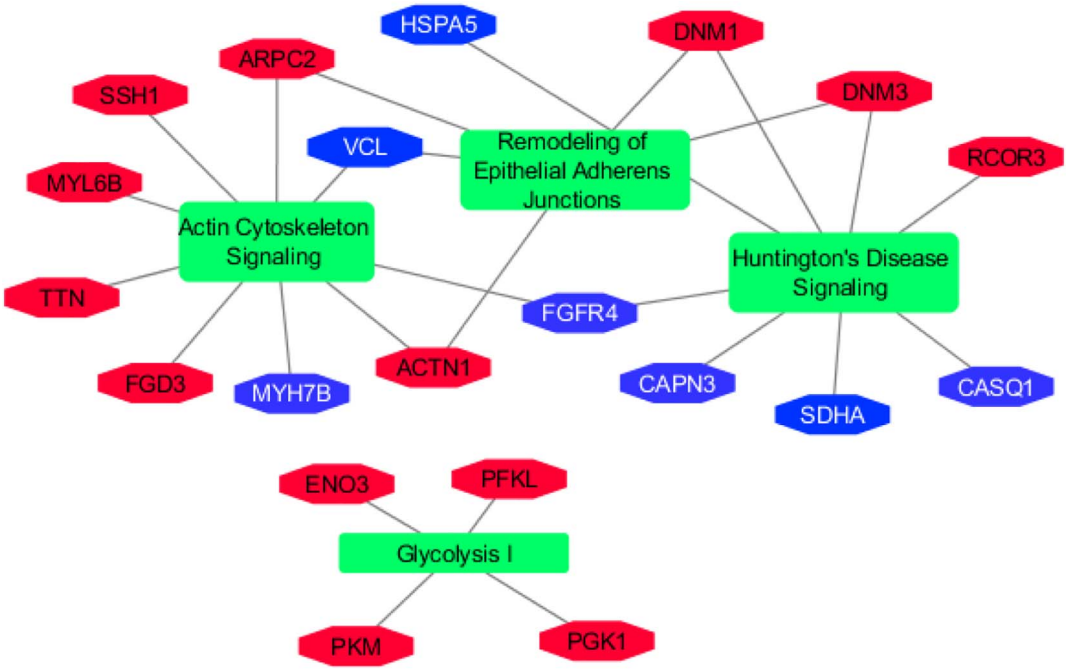

Fig. 3. Canonical pathways enriched from the list of differentially abundant proteins between High vs. Low groups based on genomic estimated breeding values for intramuscular fat by Ingenuity Pathway Analysis [IPA]. The shapes in green represent the pathways enriched, the blue shapes represent the up-regulated proteins in the High group, and red shapes represent the down-regulated proteins in the High group. (For interpretation of the references to colour in this figure legend, the reader is referred to the web version of this article.)

protein abundance for the *DIS3L* and *DPYSL2* genes in H and L groups, respectively. For the *LRRFIP1* gene, miRNA expression could not explain the discrepancy between mRNA and protein level, since none of the DE miRNAs had *LRRFIP1* as a target gene.

To better understand the biological processes involved in IMF deposition the functional enrichment was performed from three different lists by DAVID software: (1) the list containing just the DEGs; (2) the list containing just the DAPs; and (3) the list containing the DEGs plus the DAPs. These results showed that the biological processes, such as sarcomere organization (GO:0045214) and intracellular signal transduction (GO:0035556), and the KEGG pathway of regulation of actin cytoskeleton (bta04810) were enriched for both lists of DEGs and DAPs (Supplementary Table S7, *Data in Brief* article). We also observed that some proteins were involved in the same biological processes and metabolic pathways when we used the list containing just the DEGs or the list containing the DEGs plus the DAPs (Supplementary Table S8, *Data in Brief* article). In agreement with IPA enrichment results, insulin resistance, MAPK signaling and actin cytoskeleton regulation pathways, as well as cell-cell adherens junction (cellular component) were also found. Besides, DAPs were enriched for GO terms and metabolic pathways divergent from those found for DEGs, such as carbon metabolism (bta01200) and glycolysis/gluconeogenesis (bta00010) (Supplementary Table S9 and S10, *Data in Brief* article).

4. Discussion

Understanding the molecular mechanisms related to fat deposition in *Longissimus dorsi* muscle is key to improve our understanding of metabolic disease, sensory characteristics and nutritional value of beef. Previous research in LD muscle of *Bos indicus* observed similar concentrations of IMF as described here, ranging from 1.5 to 4% IMF in Nelore cattle [51,52]. In this study, animals of the similar age and the same breed, sex, and fed the same diet had different average of IMF content between groups, indicating that this may be due to genetic variation among animals.

Recent advances in proteomic methodologies have allowed a higher proteome coverage and greater confidence in protein and peptide identification in complex biological samples, such as skeletal muscle

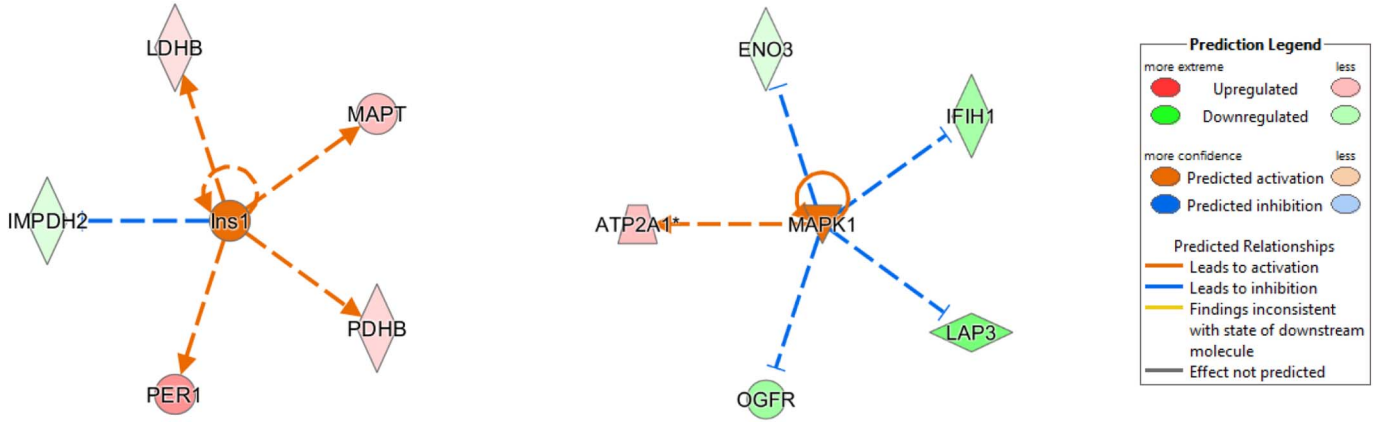

Fig. 4. Differentially abundant proteins between High vs. Low groups based on genomic estimated breeding values for intramuscular fat regulated by *Insulin 1* and *MAPK1* upstream regulators predicted as activated by Ingenuity Pathway Analysis [IPA]. Prediction legend shows the meaning of the colors schemes of shapes and connecting lines.

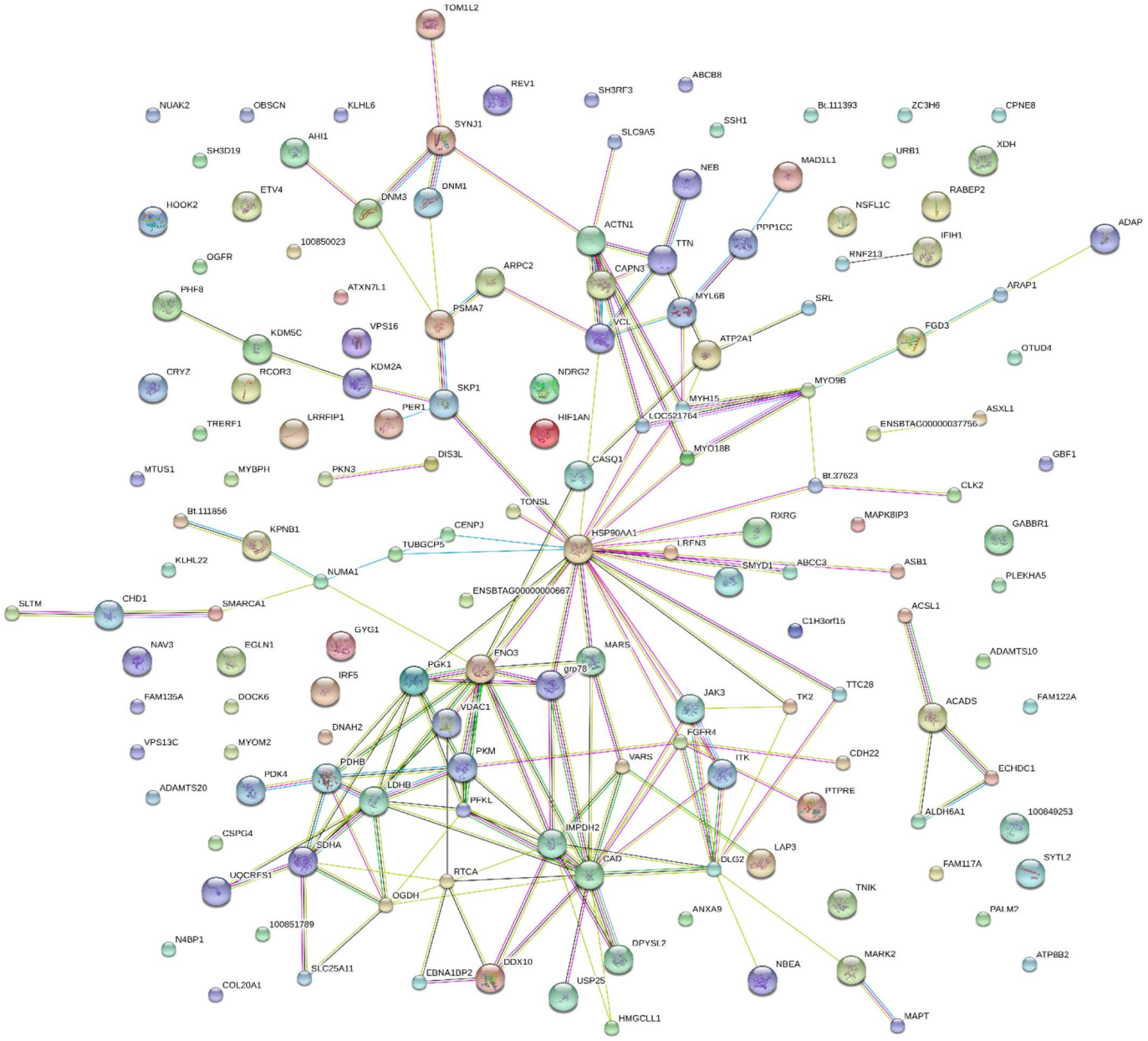

Fig. 5. Network of predicted protein-protein interactions against *Bos taurus* database from differentially abundant proteins between High vs. Low groups based on genomic estimated breeding values for intramuscular fat was constructed by STRING 10.0 online software. The network nodes are proteins and the edges represent the predicted functional associations. Each colored lines represent different evidences for each interaction: red, fusion; green, neighborhood; blue, co-occurrence; purple, experimental; yellow, text mining; light blue, database; black, co-expression. (For interpretation of the references to colour in this figure legend, the reader is referred to the web version of this article.)

tissue. Our study identified a higher number of proteins (2529) in the LD muscle using label-free multidimensional nanoUPLC-HDMSE coupled with protein database generated by transcriptome analysis in comparison to previous studies [16,17,19,51,53]. The use of transcriptome database to construct a protein database to identify peptides detected by mass spectrometry have been reported in some studies [54,55], with clear benefits for the identification of several distinct proteins in a single experiment and better quality of genome functional annotation [56].

We identified 164 differentially abundant proteins (p-value < 0.05) between the two groups for intramuscular fat deposition in Nelore steers. Eight-three proteins were down-regulated and 81 up-regulated in H group. The most prominent up-regulated proteins in H IMF group were FAM135A (FC = 2.95) and PLEKHA5 (FC = 2.80). FAM135A protein is involved in the cellular lipid metabolic process, and PLEKHA5 interacts with phosphoinositides (PI3P, PI4P, PI5P and PI (3,5)P2) and targets proteins to the membrane due to its PH (pleckstrin homology) domain [57]. PLEKHA5 has been associated with intracellular signaling and cytoskeletal organization [58]. Phosphoinositides are an important family of lipids present in eukaryotic cells and responsible for regulating vesicular traffic and modulating lipid distribution and metabolism [59].

The lowest fold change estimate was found for Copine-8 (down regulated in H IMF group). This protein is a calcium-dependent phospholipid binding protein involved in membrane trafficking phenomena [60,61]. Moreover, copines have demonstrated the ability to recruit other target proteins to the membrane surface, mainly proteins that are involved in intracellular signal transduction pathways [62]. Similar to the copines, the annexins and synaptotagmin, which were also found to be down-regulated in the H IMF group, have broad importance in the assembly of proteins from cytosol to membrane surfaces involving calcium-dependent regulation [62].

Table 3
Differentially expressed genes corresponding to differentially abundant proteins in both transcriptomic and proteomic analyses [p-value < 0.05] between High vs. Low groups based on genomic estimated breeding values for intramuscular fat percentage from *Longissimus dorsi* muscle.

Ensembl ID	Gene name	Uniprot ID	Description	Log2FC[a]	
				mRNA	Protein
ENSBTAG00000018255	*ACTN1*	P05094	Alpha-actinin-1	−0.40	−1.48
ENSBTAG00000014207	*Adamts10*	P58459	A disintegrin and metalloproteinase with thrombospondin motifs 10	−0.34	−0.37
ENSBTAG00000000667	*APOL3*	O95236	Apolipoprotein L3	−0.87	−0.34
ENSBTAG00000000371	*DIS3L*	A0JN80	DIS3-like exonuclease 1	0.31	−1.73
ENSBTAG00000018373	*DPYSL2*	O02675	Dihydropyrimidinase-related protein 2 [DRP-2]	−0.31	1.85
ENSBTAG00000006270	*HSP90AA1*	Q76LV2	Heat shock protein HSP 90-alpha	−0.22	−0.50
ENSBTAG00000037951	*KLHL6*	Q8WZ60	Kelch-like protein 6	−0.93	−0.23
ENSBTAG00000005354	*Lrrfip1*	Q3UZ39	Leucine-rich repeat flightless-interacting protein 1	−0.46	0.21
ENSBTAG00000039682	*MTUS1*	Q5R9I1	Microtubule-associated tumor suppressor 1 homolog	0.33	2.17
ENSBTAG00000011465	*MYBPH*	Q13203	Myosin-binding protein H	−1.79	−0.56
ENSBTAG00000000698	*MYO18B*	Q8IUG5	Unconventional myosin-XVIIIb	−0.33	−1.03
ENSBTAG00000010195	*PKN3*	Q6P5Z2	Serine/threonine-protein kinase N3	−0.55	−0.34
ENSBTAG00000017233	*RNF213*	Q63HN8	E3 ubiquitin-protein ligase RNF213	−1.11	−1.11
–	*SRL*	P13666	Sarcalumenin	1.57	0.41
ENSBTAG00000000460	*SYTL2*	A6QP06	Synaptotagmin-like protein 2	−0.42	−0.56
ENSBTAG00000019314	*USP25*	Q9UHP3	Ubiquitin carboxyl-terminal hydrolase 25	0.31	0.57
–	*ZC3H6*	P61129	Zinc finger CCCH domain-containing protein 6	0.60	0.39

[a] Fold Change [log2] High:Low.

One significant canonical pathway identified was glycolysis. There were four proteins, Enolase 3 (ENO3), ATP-dependent 6-phosphofructokinase (PFKL), phosphoglycerate kinase 1 (PGK1), and Pyruvate kinase (PKM) with lower abundance in H group. These results were consistent with another study, which also demonstrated that two proteins related to glycolysis, PGK1 e triosephosphate isomerase (TPI1), were down-regulated in the High-fat group of Xiangxi yellow x Angus crossbred cattle [12]. Therefore, appears that a decreased of glycolytic enzymes is associated with intramuscular fat accumulation. However, PGK1 was found in lower abundance in LD muscle from low marbling score group in Hanwoo cattle [11]. Nevertheless, glycolytic proteins as ENO3, PKM2, and GPI (glucose-6-phosphate isomerase) were found in higher abundance in *Longissimus lumborum* muscle from Aberdeen Angus sires steers with high intramuscular fat content [13].

The primary substrate for fat synthesis in ruminants is acetate derived from fermentation in the rumen, but there is also evidence that intramuscular adipocytes use glucose/lactate as a source of acetyl units for lipogenesis [63]. Among the up-regulated proteins in H group were L-lactate dehydrogenase B chain (LDHB), which catalyze the interconversion of pyruvate and lactate, and Pyruvate dehydrogenase E1 (PDHB), which transform pyruvate into Acetyl-CoA, facilitating fat synthesis in skeletal muscle. The utilization of lactate as a carbon source for fatty acids synthesis in bovine adipose tissue has already been reported [64]. Recently, lactate has been described as a primary source of carbon for the tricarboxylic acid (TCA) cycle in mice [65]. Moreover, Pyruvate dehydrogenase kinase isozyme 4 (PDK4), a kinase that inhibits pyruvate dehydrogenase activity, and thereby regulates metabolite flux through the TCA cycle, was down regulated in H group. Therefore, although these findings are not surprising, glycolytic metabolism and the use of lactate as a source for marbling synthesis remains unclear and merits further investigation.

Proteins from TCA cycle, such as Short-chain specific acyl-CoA dehydrogenase (ACADS), 2-oxoglutarate dehydrogenase (OGDH), and Succinate dehydrogenase [ubiquinone] flavoprotein subunit (SDHA) were in higher abundances in the H group. The presence of Acetyl-CoA and reduced form of nicotinamide adenine dinucleotide phosphate (NADPH) is required for fatty acid synthesis [66]. Acetyl-CoA combines with oxaloacetate from TCA cycle to produce citrate, which is transported to the cytoplasm and used in the fatty acid synthesis [67]. A previous study reported higher abundance of Aconitase 2 and OGDH in Aberdeen Angus compared with Belgian Blue steers, which are contrasting for adiposity [13]. However, succinate dehydrogenase is more abundant in early versus late-fattening stage in Korean cattle [14].

Pathways related to cellular junctions and actin cytoskeleton signaling may contribute to IMF deposition. Most of the actin-binding proteins (ACTN1, ARPC2, SSH1, TTN) was down-regulated in the H IMF group, suggesting a cellular rearrangement to make space for the adipocyte. Decreased expression of actin, tubulin, integrin and other cytoskeletal proteins are very early events in adipocyte differentiation [68,69]. Adipocytes differentiation causes a significant change in cellular shape, resulting in the epithelial remodeling of the extracellular matrix (ECM) and actin cytoskeleton rearrangements [4,70]. Alterations in cytoskeleton organization and cell junctions have been shown to participate in the accumulation of IMF during chicken development [71]. Taye et al. [72] studying meat quality parameters, including IMF deposition in Ankole cattle breed identified gene ontology terms of cellular component organization and actin cytoskeleton involved in adipocyte regulation, supporting our findings.

Moreover, our results revealed structural proteins differentially abundant between groups. Myosin-15 (MYH15), Myosin light chain 6B (MYL6B), and Titin (TTN) had decreased abundance in H group, while Myosin 7B (MYH7B), and Nebulin (NEB) increased. Reduced abundance of structural proteins has already been reported in high-fat group animals in others proteomics studies [12,15]. Therefore, these findings confirm changes in muscle structure during adipogenesis.

Additionally, IPA upstream regulator analysis predicted Ins1 and MAPK1 pathways as significantly activated upstream regulators in our *Longissimus dorsi* muscle samples. Insulin signaling plays a pivotal role in maintaining basic cellular functions such as synthesis and degradation of glycogen, lipids, and proteins [73], and insulin resistance has been linked to lipid accumulation in skeletal muscle and consequently associated with metabolic diseases such as obesity [74]. Another important pathway that controls insulin resistance is MAPK, an intracellular signaling pathway that plays a key role in cellular processes of proliferation and differentiation [75] Several studies have associated the role of MAPKs in the regulation of lipid metabolism [76–79].

Heat shock protein 90 alpha (HSP90AA1) was shown as central core of network predicted by STRING and down-regulated in LD muscle of animals with High values of intramuscular fat content. HSP90 is a chaperone essential for cell growth and survival [80]. HSP90 interacts with several proteins including kinases, nuclear receptors, and transcription factors [81]. Recently, HSP90 has been identified to regulate lipid metabolism by controlling SCAP/SREBP (SREBP cleavage-activating protein/sterol regulatory element-binding proteins) complex

Table 4
Expression level of differentially expressed microRNAs [p < 0.05] between High vs. Low groups for intramuscular fat that targets DIS3L and DPYSL2 genes, and partial correlation coefficient values obtained from microRNAs expression and protein abundance. The microRNAs more representative to explain differences in mRNA expression and protein abundance are highlighted in bold.

microRNAs target DIS3L	microRNAs expression		microRNA-protein correlation	
	H	L	H	L
bta_let_7a_5p	**1908.20**	1526.04	0.16	−0.52
bta_let_7e	**118.23**	70.99	0.10	−0.36
bta_miR_100	840.72	1968.02	0.34	−0.19
bta_miR_1388_5p	59.64	63.43	−0.05	0.87
bta_miR_143	27,539.78	32,275.17	0.71	−0.26
bta_miR_2284x	**55.35**	48.45	0.51	−0.25
bta_miR_2284y	**55.35**	48.45	0.51	−0.25
bta_miR_30a_5p	12,141.64	13,282.18	0.43	−0.12
bta_miR_339a	**71.51**	57.20	**−0.25**	0.44
bta_miR_339b	**71.51**	57.20	**−0.25**	0.44
bta_miR_376e	0.12	0.80	−0.26	0.07
bta_miR_423_5p	**488.05**	311.91	**−0.18**	0.08
bta_miR_454	0.54	2.07	−0.02	−0.09
bta_miR_504	**25.82**	21.21	0.46	0.48
bta_miR_665	4.27	6.99	−0.28	−0.32
bta_miR_874	16.49	22.40	−0.25	0.46

microRNAs target DPYSL2	microRNAs expression		microRNA-protein correlation	
	H	L	H	L
bta_let_7a_5p	1908.20	1526.04	−0.20	0.21
bta_let_7e	118.23	70.99	0.35	−0.41
bta_miR_1271	13.86	**42.14**	−0.45	0.10
bta_miR_1388_5p	59.64	**63.43**	−0.36	**−0.42**
bta_miR_143	27,539.78	**32,275.17**	0.14	**−0.44**
bta_miR_222	8.47	4.70	−0.25	0.24
bta_miR_22_3p	11,510.50	9426.42	0.66	−0.34
bta_miR_2284x	55.35	48.45	0.63	−0.37
bta_miR_2284y	55.35	48.45	0.63	−0.37
bta_miR_30a_5p	12,141.64	**13,282.18**	0.16	**−0.38**
bta_miR_30c	610.48	526.56	−0.07	0.77
bta_miR_324	0.08	**0.71**	−0.10	0.04
bta_miR_339a	71.51	57.20	−0.17	0.07
bta_miR_339b	71.51	57.20	−0.17	0.07
bta_miR_376e	0.12	**0.80**	−0.04	0.22
bta_miR_423_5p	488.05	311.91	0.16	−0.01
bta_miR_454	0.54	**2.07**	−0.05	0.16
bta_miR_487b	5.26	3.55	0.13	0.54
bta_miR_504	25.82	21.21	−0.17	−0.06
bta_miR_874	16.49	**22.40**	−0.17	**−0.36**
bta_miR_98	141.73	105.68	0.20	0.35

proteins [82]. The SREBPs are key transcription factors that modulate the transcription of a range of lipogenic enzymes [83]. Other members of the heat shock protein family (72 and 27) play a protective role in insulin resistance in monocytes from obese patients via inhibition of key stress kinases [84]. This suggests that decreased expression of heat shock proteins may lead to greater fat deposition.

A comparative analysis between transcriptomic (mRNA) and proteomic data allowed us to investigate the relationship between mRNA expression level and protein abundance. Out of the 17 DAPs that were also DE at the transcript level, we found a direct mRNA/protein relationship for 14 genes and to unravel two of the three unexpected mRNA/protein relationship by miRNA data. The relation of mRNA expression with protein expression is influenced by several post-transcriptional regulatory mechanisms [85]. Among them are miRNAs that bind in mRNA and can degrade mRNAs and suppress translation [86].

Previous reports also demonstrated divergent results between transcriptomic and proteomic data. In an integrative analysis of transcriptomic and proteomic of skeletal muscle from pigs, only three genes were found to be differentially expressed at the protein and mRNA level [87]. Analysis of liver from Chianina and Holstein Friesian cattle validated only three proteins of 39 differentially abundant by microarray analysis [88]. However, no previous studies have used miRNAs to explain mRNA/protein relationship.

Apolipoprotein L3 (APOL3), HSP90AA1, Zinc finger CCCH domain-containing protein 6 (ZC3H6), and RNF213-E3 ubiquitin-protein ligase (RNF213) agreed in fold change direction for protein and mRNA, and are potential candidates for IMF deposition.

Apolipoproteins are involved in the transport of lipids in the cytoplasm, including cholesterol, and may allow the binding of lipids to organelles [89]. We found APOL3 mRNA and protein down-regulated in H group. APOL3 was identified as a highly duplicate gene in the beef breeds, revealing higher copy number of this gene in Angus animals compared with Holstein, Hereford, and Nelore [90]. Furthermore, another type of Apolipoprotein has already been reported in lipid droplet proteome in rat skeletal muscle [91]. Therefore, APOL3 gene appears to be a candidate gene for IMF deposition.

Two zinc finger proteins, Zinc finger-containing CCCH domain-containing protein 6 (ZC3H6) and Protein ZGRF1 (ZGRF1), were identified in this study in higher abundance in the H group: The first one also showed higher mRNA expression in H group. Zinc finger

proteins (ZFPs) family act by controlling the differentiation of mesenchymal stem cells into myogenic, adipogenic or osteogenic cells [66]. ZFPs are one of the largest classes of transcription factors present in the eukaryotic genome, regulating various processes such as cell proliferation, growth, differentiation, metabolism, immunity, and adipogenesis through DNA/RNA binding, protein-protein interactions, transcription activation and apoptosis [92]. Some ZFPs have already been described as participants in the adipogenesis process, such as Zfp423, Zfp467, Zfp52 and ZNF396 [92].

RNF213 (E3 ubiquitin-protein ligase RNF213) is a protein characterized by the presence of a RING finger domain, a type of specialized zinc finger domain. This protein is involved in angiogenesis [93], in the protein ubiquitination pathway and the negative regulation of the non-canonical Wnt signaling pathway [94]. The Wnt signaling pathway, once activated, restricts adipogenesis by inhibiting the expression of PPARγ and CEPA (CCAAT/enhancer-binding protein-α), central transcriptional regulators of adipogenesis [95]. On the other hand, the role of the non-canonical Wnt pathway is to antagonize the effects of the canonical pathway, promoting adipogenesis. These reports agree with our finds, where higher mRNA and protein levels of RNF213 were detected in the group with lower IMF deposition.

Although the proteomic and transcriptomic results had limited overlap, functional enrichment analysis demonstrated that biological processes and metabolic pathways were shared between DEGs and DAPs, especially regulation of actin cytoskeleton and cell-cell adherens junction and pathways for MAPK and insulin. Moreover, proteomic data complemented transcriptomic study with proteins found to be involved in glycolysis metabolism. The integrative analysis provided a deeper understanding of complex biological processes associated with intramuscular fat deposition.

5. Conclusions

The results demonstrated that proteins involved in glycolysis metabolism, actin cytoskeleton signaling, cell-cell adherens junction and pathways for MAPK and insulin are important biological mechanisms involved in bovine LD muscle IMF deposition. Particularly, lactate appears to be an important source of carbon for fat deposition in ruminants. In addition, the overall transcriptome and proteome changes associated with IMF demonstrated that sarcomere organization, intracellular signal transduction and regulation of actin cytoskeleton are mechanisms altered for IMF deposition. The integration of mRNA, miRNA and protein levels allowed us to better understand the relationship between expression of mRNAs and proteins. These findings provide a deeper understanding of the highly complex regulatory mechanisms involved in IMF deposition in cattle.

Nomenclature

IMF	intramuscular fat
HDMS^E	High Definition Mass Spectrometry
GEBV	genomic estimated breeding values
LD	*Longissimus dorsi*
BFT	backfat thickness
REA	ribeye area
GBLUP	genomic best linear unbiased prediction
DAP	differentially abundant proteins
DEG	differentially expressed genes

Author contributions

The manuscript was written through contributions of all authors. MDP drafted the manuscript. MDP, RCS and GHMFS participated in the experimental design. MDP, GHMFS, ASMC, BSV and LLC collaborated with interpretation and discussion of the results. ASMC provided the mRNA data. GBO provided the microRNA data. SCSA provided the transcriptomic database. LCAR, LLC and LCC provided the experimental environment and coordination. All authors have given approval to the final version of the manuscript.

Funding sources

This study was conducted with funding from EMBRAPA (Macroprograma 1, 01/2005) and São Paulo Research Foundation (FAPESP processes number 2012/23638-8 and 2013/21017-9). LCAR and LLC were granted CNPq fellowships.

Conflict of interest

The authors declare that they have no conflict of interest.

Acknowledgments

The authors acknowledge the São Paulo Research Foundation for providing scholarship (FAPESP 2013/21017-9) to Mirele Daiana Poleti and financial support for research (FAPESP2012/23638-8). We also acknowledge the University of São Paulo; Federal University of State of Rio de Janeiro (UNIRIO); EMBRAPA; Comitê Olímpico do Brasil (BOC); Conselho Nacional de Desenvolvimento Científico e Tecnológico (CNPq); Coordenação de Aperfeiçoamento de Pessoal de Nível Superior (CAPES); Financiadora de Estudos e Projetos (FINEP); Fundação Carlos Chagas Filho de Amparo à Pesquisa do Estado do Rio de Janeiro (FAPERJ); Merck-Sigma-Aldrich; and Waters Corporation for the collaborative efforts.

References

[1] N. Scollan, J.F. Hocquette, K. Nuernberg, D. Dannenberger, I. Richardson, A. Moloney, Innovations in beef production systems that enhance the nutritional and health value of beef lipids and their relationship with meat quality, Meat Sci. 74 (1) (2006) 17–33.
[2] M.V. Dodson, Z. Jiang, J. Chen, G.J. Hausman, L.L. Guan, J. Novakofski, D.P. Thompson, C.L. Lorenzen, M.E. Fernyhough, P.S. Mir, J.M. Reecy, Allied industry approaches to alter intramuscular fat content and composition in beef animals, J. Food Sci. 75 (1) (2010) R1–8.
[3] J.D. Wood, M. Enser, A.V. Fisher, G.R. Nute, P.R. Sheard, R.I. Richardson, S.I. Hughes, F.M. Whittington, Fat deposition, fatty acid composition and meat quality: a review, Meat Sci. 78 (4) (2008) 343–358.
[4] M. Bonnet, I. Cassar-Malek, Y. Chilliard, B. Picard, Ontogenesis of muscle and adipose tissues and their interactions in ruminant and other species, Animal 4 (7) (2010) 1093–1109.
[5] J.F. Hocquette, F. Gondret, E. Baéza, F. Médale, C. Jurie, D.W. Pethick, Intramuscular fat content in meat-producing animals: development, genetic and nutritional control, and identification of putative markers, Animal 4 (2) (2010) 303–319.
[6] A.S. Cesar, L.C. Regitano, J.E. Koltes, E.R. Fritz-Waters, D.P. Lanna, G. Gasparin, G.B. Mourão, P.S. Oliveira, J.M. Reecy, L.L. Coutinho, Putative regulatory factors associated with intramuscular fat content, PLoS One 10 (6) (2015) e0128350.
[7] S.C. Shin, E.R. Chung, Identification of differentially expressed genes between high and low marbling score grades of the longissimus lumborum muscle in Hanwoo (Korean cattle), Meat Sci. 121 (2016) 114–118.
[8] B. Soret, J.A. Mendizabal, A. Arana, L. Alfonso, Expression of genes involved in adipogenesis and lipid metabolism in subcutaneous adipose tissue and longissimus muscle in low-marbled Pirenaica beef cattle, Animal 10 (12) (2016) 2018–2026.
[9] B. Schwanhäusser, D. Busse, N. Li, G. Dittmar, J. Schuchhardt, J. Wolf, W. Chen, M. Selbach, Global quantification of mammalian gene expression control, Nature 473 (7347) (2011) 337–342.
[10] C. Vogel, R.S. Abreu, D. Ko, S.-Y. Le, B.A. Shapiro, S.C. Burns, D. Sandhu, D.R. Boutz, E.M. Marcotte, L.O. Penalva, Sequence signatures and mRNA concentration can explain two-thirds of protein abundance variation in a human cell line, Mol. Syst. Biol. 6 (2010) 400.
[11] Y.N. Shen, S.H. Kim, D.H. Yoon, H.G. Lee, H.S. Kang, K.S. Seo, Proteome analysis of bovine longissimus dorsi muscle associated with the marbling score, Asian Australas. J. Anim. Sci. 25 (8) (2012) 1083–1088.
[12] Y. Mao, D.L. Hopkins, Y. Zhang, P. Li, L. Zhu, P. Dong, R. Liang, J. Dai, X. Wang, X. Luo, Beef quality with different intramuscular fat content and proteomic analysis using isobaric tag for relative and absolute quantitation of differentially expressed proteins, Meat Sci. 118 (2016) 96–102.
[13] S.M. Keady, D.A. Kenny, K. Ohlendieck, S. Doyle, M.G. Keane, S.M. Waters, Proteomic profiling of bovine M. Longissimus lumborum from crossbred Aberdeen Angus and Belgian blue sired steers varying in genetic merit for carcass weight, J. Anim. Sci. 91 (2013) 654–665.

[14] N.K. Kim, S.H. Lee, Y.M. Cho, E.S. Son, K.Y. Kim, C.S. Lee, D. Yoon, S.K. Im, S.J. Oh, E.W. Park, Proteome analysis of the m. Longissimus dorsi between fattening stages in Hanwoo steer, BMB Rep. 42 (7) (2009) 4333–4338.
[15] Q. Zhang, H.G. Lee, J.A. Han, E.B. Kim, S.K. Kang, J. Yin, M. Baik, Y. Shen, S.H. Kim, K.S. Seo, Y.J. Choi, Differentially expressed proteins during fat accumulation in bovine skeletal muscle, Meat Sci. 86 (3) (2010) 814–820.
[16] J. Bouley, B. Meunier, C. Chambon, S. De Smet, J.F. Hocquette, B. Picard, Proteomic analysis of bovine skeletal muscle hypertrophy, Proteomics 5 (2) (2005) 490–500.
[17] M.E. Carvalho, G. Gasparin, M.D. Poleti, A.F. Rosa, J.C. Balieiro, C.A. Labate, R.T. Nassu, R.R. Tullio, L.C. Regitano, G.B. Mourão, L.L. Coutinho, Heat shock and structural proteins associated with meat tenderness in Nelore beef cattle, a Bos indicus breed, Meat Sci. 96 (3) (2014) 1318–1324.
[18] D. Franco, A. Mato, F.J. Salgado, M. López-Pedrouso, M. Carrera, S. Bravo, M. Parrado, J.M. Gallardo, C. Zapata, Tackling proteome changes in the longissimus thoracis bovine muscle in response to pre-slaughter stress, J. Proteome 122 (2015) 73–85.
[19] X. Jia, K.I. Hildrum, F. Westad, E. Kummen, L. Aass, K. Hollung, Changes in enzymes associated with energy metabolism during the early post mortem period in longissimus thoracis bovine muscle analyzed by proteomics, J. Proteome Res. 5 (7) (2006) 1763–1769.
[20] P.D. Eckersall, A.M. de Almeida, I. Miller, Proteomics, a new tool for farm animal science, J. Proteome 75 (14) (2012) 4187–4189.
[21] A. D'Alessandro, L. Zolla, Meat science: from proteomics to integrated omics towards system biology, J. Proteome 78 (2013) 558–577.
[22] C. Ramus, A. Hovasse, M. Marcellin, A.M. Hesse, E. Mouton-Barbosa, D. Bouyssié, S. Vaca, C. Carapito, K. Chaoui, C. Bruley, J. Garin, S. Cianférani, M. Ferro, A. Van Dorssaeler, O. Burlet-Schiltz, C. Schaeffer, Y. Couté, A. Gonzalez de Peredo, Benchmarking quantitative label-free LC-MS data processing workflows using a complex spiked proteomic standard dataset, J. Proteome 132 (2016) 51–62.
[23] N.J. Bond, P.V. Shliaha, K.S. Lilley, L. Gatto, Improving qualitative and quantitative performance for MS[E]-based label-free proteomics, J. Proteome Res. 12 (6) (2013) 2340–2353.
[24] G.B. Oliveira, L.C.A. Regitano, A.S.M. Cesar, J.M. Reecy, K.Y. Degaki, M.D. Poleti, A.M. Felicio, J.E. Koltes, L.L. Coutinho, Integrative analysis of microRNAs and mRNAs revealed regulation of composition and metabolism in Nelore cattle, BMC Genomics 19 (2018) 126.
[25] P.C. Tizioto, J.E. Decker, J.F. Taylor, R.D. Schnabel, M.A. Mudadu, F.L. Silva, G.B. Mourão, L.L. Coutinho, P. Tholon, T.S. Sonstegard, A.N. Rosa, M.M. Alencar, R.R. Tullio, S.R. Medeiros, R.T. Nassu, G.L. Feijó, L.O. Silva, R.A. Torres, F. Siqueira, R.H. Higa, L.C. Regitano, Genome scan for meat quality traits in Nelore beef cattle, Physiol. Genomics 45 (21) (2013) 1012–1020.
[26] Gilmour AR, B.J. Gogel, B.R. Cullis, S.J. Welham, R. Thompson, ASReml User Guide Release 3.0, VSN International Ltd: Hemel Hempstead, HP1 1ES, UK, (2009).
[27] Y.Q. Yu, M. Gilar, P.J. Lee, E.S. Bouvier, J.C. Gebler, Enzyme-friendly, mass spectrometry-compatible surfactant for in-solution enzymatic digestion of proteins, Anal. Chem. 75 (21) (2003) 6023–6028.
[28] M. Gilar, P. Olivova, A.E. Daly, J.C. Gebler, Two-dimensional separation of peptides using RP-RP-HPLC system with different pH in first and second separation dimensions, J. Sep. Sci. 28 (14) (2005) 1694–1703.
[29] P.M. Lalli, Y.E. Corilo, M. Fasciotti, M.F. Riccio, G.F. de Sa, R.J. Daroda, G.H. Souza, M. McCullagh, M.D. Bartberger, M.N. Eberlin, I.D. Campuzano, Baseline resolution of isomers by traveling wave ion mobility mass spectrometry: investigating the effects of polarizable drift gases and ionic charge distribution, J. Mass Spectrom. 48 (9) (2013) 989–997.
[30] W.M. Silva, R.D. Carvalho, S.C. Soares, I.F. Bastos, E.L. Folador, G.H. Souza, Y. Le Loir, A. Miyoshi, A. Silva, V. Azevedo, Label-free proteomic analysis to confirm the predicted proteome of Corynebacterium pseudotuberculosis under nitrosative stress mediated by nitric oxide, BMC Genomics 15 (2014) 1065.
[31] S.J. Geromanos, J.P. Vissers, J.C. Silva, C.A. Dorschel, G.Z. Li, M.V. Gorenstein, R.H. Bateman, J.I. Langridge, The detection, correlation, and comparison of peptide precursor and product ions from data independent LC-MS with data dependant LC-MS/MS, Proteomics 9 (6) (2009) 1683–1695.
[32] W.M. Silva, E.L. Folador, S.C. Soares, G. Souza, A.V. Santos, C.S. Sousa, H. Figueiredo, A. Miyoshi, Y. Le Loir, A. Silva, V. Azevedo, Label-free quantitative proteomics of Corynebacterium pseudotuberculosis isolates reveals differences between Biovars ovis and equi strains, BMC Genomics 18 (2017) 451.
[33] M.D. Lobo, F.B. Moreno, G.H. Souza, S.M. Verde, R.A. Moreira, A.C. Monteiro-Moreira, Label-free proteome analysis of plasma from patients with breast cancer: stage-specific protein expression, Front. Oncol. 7 (2017) 14.
[34] W.M. Silva, F.A. Dorella, S.C. Soares, G.H. Souza, T.L. Castro, N. Seyffert, H. Figueiredo, A. Miyoshi, Y. Le Loir, A. Silva, V. Azevedo, A shift in the virulence potential of Corynebacterium pseudotuberculosis biovar ovis after passage in a murine host demonstrated through comparative proteomics, BMC Microbiol. 17 (1) (2017) 55.
[35] G.W.P. Neves, N. Curty, P.H. Kubitschek-Barreira, T. Fontaine, G. Souza, M.L. Cunha, G.H. Goldman, A. Beauvais, J.P. Latgé, L.M. Lopes-Bezerra, Dataset of differentially regulated proteins in HUVECs challenged with wild type and UGM1 mutant aspergillus fumigatus strains, Data Brief 9 (2016) 24–31.
[36] A.S. Heringer, T. Barroso, A.F. Macedo, C. Santa-Catarina, G.H. Souza, E.I. Floh, G.A. de Souza-Filho, V. Silveira, Label-free quantitative proteomics of embryogenic and non-embryogenic callus during sugarcane somatic embryogenesis, PLoS One 10 (6) (2015) e0127803.
[37] J.C. Silva, M.V. Gorenstein, G.Z. Li, J.P. Vissers, S.J. Geromanos, Absolute quantification of proteins by LCMSE: a virtue of parallel MS acquisition, Mol. Cell. Proteomics 5 (1) (2006) 144–156.
[38] J.C. Silva, R. Denny, C.A. Dorschel, M. Gorenstein, I.J. Kass, G.Z. Li, T. McKenna, M.J. Nold, K. Richardson, P. Young, S. Geromanos, Quantitative proteomic analysis by accurate mass retention time pairs, Anal. Chem. 77 (7) (2005) 2187–2200.
[39] G.H. Souza, P.C. Guest, D. Martins-de-Souza, LC-MSE, multiplex MS/MS, ion mobility, and label-free quantitation in clinical proteomics, Methods Mol. Biol. 1546 (2017) 57–73.
[40] A. Reverter, E.K. Chan, Combining partial correlation and an information theory approach to the reversed engineering of gene co-expression networks, Bioinformatics 24 (21) (2008) 2491–2497.
[41] M.G. Grabherr, B.J. Haas, M. Yassour, J.Z. Levin, D.A. Thompson, I. Amit, X. Adiconis, L. Fan, R. Raychowdhury, Q. Zeng, Z. Chen, E. Mauceli, N. Hacohen, A. Gnirke, N. Rhind, F. di Palma, B.W. Birren, C. Nusbaum, K. Lindblad-Toh, N. Friedman, A. Regev, Full-length transcriptome assembly from RNA-Seq data without a reference genome, Nat. Biotechnol. 29 (7) (2011) 644–652.
[42] B.J. Haas, A. Papanicolaou, M. Yassour, M. Grabherr, P.D. Blood, J. Bowden, M.B. Couger, D. Eccles, B. Li, M. Lieber, M.D. Macmanes, M. Ott, J. Orvis, N. Pochet, F. Strozzi, N. Weeks, R. Westerman, T. William, C.N. Dewey, R. Henschel, R.D. Leduc, N. Friedman, A. Regev, De novo transcript sequence reconstruction from RNA-seq using the trinity platform for reference generation and analysis, Nat. Protoc. 8 (8) (2013) 1494–1512.
[43] L. Fu, B. Niu, Z. Zhu, S. Wu, W. Li, CD-HIT: accelerated for clustering the next-generation sequencing data, Bioinformatics 28 (23) (2012) 3150–3152.
[44] A. Morgulis, E.M. Gertz, A.A. Schäffer, R. Agarwala, A fast and symmetric DUST implementation to mask low-complexity DNA sequences, J. Comput. Biol. 13 (5) (2006) 1028–1040.
[45] S. Maere, K. Heymans, M. Kuiper, BiNGO: a Cytoscape plugin to assess over-representation of gene ontology categories in biological networks, Bioinformatics 21 (16) (2005) 3448–3449.
[46] P. Shannon, A. Markiel, O. Ozier, N.S. Baliga, J.T. Wang, D. Ramage, N. Amin, B. Schwikowski, T. Ideker, Cytoscape: a software environment for integrated models of biomolecular interaction networks, Genome Res. 13 (11) (2003) 2498–2504.
[47] F. Supek, M. Bošnjak, N. Škunca, T. Šmuc, REVIGO summarizes and visualizes long lists of gene ontology terms, PLoS One 6 (7) (2011) e21800.
[48] D. Szklarczyk, A. Franceschini, S. Wyder, K. Forslund, D. Heller, J. Huerta-Cepas, M. Simonovic, A. Roth, A. Santos, K.P. Tsafou, M. Kuhn, P. Bork, L.J. Jensen, C. von Mering, STRING v10: protein-protein interaction networks, integrated over the tree of life, Nucleic Acids Res. 43 (2015) D447–52.
[49] W. Huang da, B.T. Sherman, R.A. Lempicki, Systematic and integrative analysis of large gene lists using DAVID bioinformatics resources, Nat. Protoc. 4 (1) (2009) 44–57.
[50] A.S. Cesar, L.C. Regitano, G.B. Mourão, R.R. Tullio, D.P. Lanna, R.T. Nassu, M.A. Mudado, P.S. Oliveira, M.L. do Nascimento, A.S. Chaves, M.M. Alencar, T.S. Sonstegard, D.J. Garrick, J.M. Reecy, L.L. Coutinho, Genome-wide association study for intramuscular fat deposition and composition in Nelore cattle, BMC Genet. 15 (2014) 39.
[51] R.T. Rodrigues, M.L. Chizzotti, C.E. Vital, M.C. Baracat-Pereira, E. Barros, K.C. Busato, R.A. Gomes, M.M. Ladeira, T.D. Martins, Differences in beef quality between Angus [Bos taurus taurus] and Nelore [Bos taurus indicus] cattle through a proteomic and Phosphoproteomic approach, PLoS One 12 (1) (2017) e0170294.
[52] P.D. Teixeira, D.M. Oliveira, M.L. Chizzotti, A. Chalfun-Junior, T.C. Coelho, M. Gionbelli, L.V. Paiva, J.R.R. Carvalho, M.M. Ladeira, Subspecies and diet affect the expression of genes involved in lipid metabolism and chemical composition of muscle in beef cattle, Meat Sci. 133 (2017) 110–118.
[53] A.M. Almeida, P. Nanni, A.M. Ferreira, C. Fortes, J. Grossman, R.J.B. Bessa, P. Costa, The longissimus thoracis muscle proteome in Alentejana bulls as affected by growth path, J. Proteome 152 (2017) 206–215.
[54] T. Luge, M. Kube, A. Freiwald, D. Meierhofer, E. Seemuller, S. Sauer, Transcriptomics assisted proteomic analysis of Nicotiana occidentalis infected by Candidatus Phytoplasma Mali strain AT, Proteomics 14 (16) (2014) 1882–1889.
[55] C. Mahadevan, A. Krishnan, G.G. Saraswathy, A. Surendran, A. Jaleel, M. Sakuntala, Transcriptome- assisted label-free quantitative proteomics analysis reveals novel insights into Piper nigrum-Phytophthora capsici Phytopathosystem, Front. Plant Sci. 7 (2016) 785.
[56] V.C. Evans, G. Barker, K.J. Heesom, J. Fan, C. Bessant, D.A. Matthews, De novo derivation of proteomes from transcriptomes for transcript and protein identification, Nat. Methods 9 (2012) 1207–1211.
[57] T. Yamada, S.I. Kawakami, N. Nakanishi, Expression of adipogenic transcription factors in adipose tissue of fattening wagyu and Holstein steers, Meat Sci. 81 (1) (2009) 86–92.
[58] M.A. Lemmon, Pleckstrin homology [PH] domains and phosphoinositides, Biochem. Soc. Symp. 74 (2007) 81–93.
[59] T. Balla, Phosphoinositides: tiny lipids with giant impact on cell regulation, Physiol. Rev. 93 (3) (2013) 1019–1137.
[60] P.V. Perestenko, A.M. Pooler, M. Noorbakhshnia, A. Gray, C. Bauccio, R.A. Jeffrey McIlhinney, Copines-1, -2, -3, -6 and -7 show different calcium-dependent intracellular membrane translocation and targeting, FEBS J. 277 (24) (2010) 5174–5189.
[61] J.L. Tomsig, C.E. Creutz, Copines: a ubiquitous family of Ca[2+]-dependent phospholipid-binding proteins, Cell. Mol. Life Sci. 59 (9) (2002) 1467–1477.
[62] C.E. Creutz, J.M. Edwardson, Organization and synergistic binding of copine I and annexin A1 on supported lipid bilayers observed by atomic force microscopy, Biochim. Biophys. Acta 1788 (9) (2009) 1950–1961.
[63] D.W. Pethick, G.S. Harper, V.H. Oddy, Growth, development and nutritional manipulation of marbling in cattle: a review, Aust. J. Exp. Agric. 44 (2004) 705–715.
[64] G.B. Whitehurst, D.C. Beitz, M.A. Pothoven, W.R. Ellison, M.H. Crump, Lactate as a precursor of fatty acids in bovine adipose tissue, J. Nutr. 108 (11) (1978)

1806–1811.
[65] S. Hui, J.M. Ghergurovich, R.J. Morscher, C. Jang, X. Teng, W. Lu, L.A. Esparza, T. Reya, Z. Le, J. Yanxiang Guo, E. White, J.D. Rabinowitz, Glucose feeds the TCA cycle via circulating lactate, Nature 551 (7678) (2017) 115–118.
[66] M.M. Ladeira, J.P. Schoonmaker, M.P. Gionbelli, J.C.O. Dias, T.R.S. Gionbelli, J.R.R. Carvalho, P.D. Teixeira, Nutrigenomics and beef quality: a review about lipogenesis, Int. J. Mol. Sci. 17 (2016) 918–938.
[67] W. Collin, Fatty acid oxidation and synthesis, DIAPEDIA, The Living Textbook of Diabetes, 2015, http://dx.doi.org/10.14496/dia.5105592814.23 (accessed 7 February 2018).
[68] B.M. Spiegelman, S.R. Farmer, Decreases in tubulin and actin gene expression prior to morphological differentiation of 3T3 adipocytes, Cell 29 (1) (1982) 53–60.
[69] J.L. Rodriguez Fernandez, A. Ben-Ze'ev, Regulation of fibronectin, integrin and cytoskeleton expression in differentiating adipocytes: inhibition by extracellular matrix and polylysine, Differentiation 42 (2) (1989) 65–74.
[70] D. Lin, T.-H. Chun, L. Kang, Adipose extracellular matrix remodeling in obesity and insulin resistance, Biochem. Pharmacol. 119 (2016) 8–16.
[71] H.-X. Cui, R.-R. Liu, G.-P. Zhao, M.-Q. Zheng, J.-L. Chen, J. Wen, Identification of differentially expressed genes and pathways for intramuscular fat deposition in pectoralis major tissues of fast-and slow-growing chickens, BMC Genomics 13 (1) (2012) 213.
[72] M. Taye, J. Kim, S.H. Yoon, W. Lee, O. Hanotte, T. Dessie, S. Kemp, O.A. Mwai, K. Caetano-Anolles, S. Cho, S.J. Oh, H.K. Lee, H. Kim, Whole genome scan reveals the genetic signature of African Ankole cattle breed and potential for higher quality beef, BMC Genet. 18 (1) (2017) 11–24.
[73] C. Lara-Castro, W.T. Garvey, Intracellular lipid accumulation in liver and muscle and the insulin resistance syndrome, Endocrinol. Metab. Clin. N. Am. 37 (4) (2008) 841–856.
[74] L.P. Turcotte, J.S. Fisher, Skeletal muscle insulin resistance: roles of fatty acid metabolism and exercise, Phys. Ther. 88 (2008) 1279–1296.
[75] F. Bost, M. Aouadi, L. Caron, B. Binetruy, The role of MAPKs in adipocyte differentiation and obesity, Biochimie 87 (1) (2005) 51–56.
[76] C. Ning, X. Wang, S. Gao, J. Mu, Y. Wang, S. Liu, J. Zhu, X. Meng, Chicory inulin ameliorates type 2 diabetes mellitus and suppresses JNK and MAPK pathways in vivo and in vitro, Mol. Nutr. Food Res. 61 (8) (2017) 1600673.
[77] G. Zhou, X. Wang, C. Yuan, D. Kang, X. Xu, J. Zhou, R. Geng, Y. Yang, Z. Yang, Y. Chen, Integrating miRNA and mRNA expression profiling uncovers miRNAs underlying fat deposition in sheep, Biomed. Res. Int. 2017 (2017) 1857580.
[78] B. Poudel, S.W. Lim, H.H. Ki, S. Nepali, Y.M. Lee, D.K. Kim, Dioscin inhibits adipogenesis through the AMPK/MAPK pathway in 3T3-L1 cells and modulates fat accumulation in obese mice, Int. J. Mol. Med. 34 (5) (2014) 1401–1408.
[79] J. Ahn, H. Lee, S. Kim, J. Park, T. Ha, The anti-obesity effect of quercetin is mediated by the AMPK and MAPK signaling pathways, Biochem. Biophys. Res. Commun. 373 (4) (2008) 545–549.
[80] F.H. Schopf, M.M. Biebl, J. Buchner, The HSP90 chaperone machinery, Nat. Rev. Mol. Cell Biol. 18 (6) (2017) 345–360.
[81] M. Taipale, D.F. Jarosz, S. Lindquist, HSP90 at the hub of protein homeostasis: emerging mechanistic insights, Nat. Rev. Mol. Cell Biol. 11 (7) (2010) 515–528.
[82] Y.C. Kuan, T. Hashidume, T. Shibata, K. Uchida, M. Shimizu, J. Inoue, R. Sato, Heat shock protein 90 modulates lipid homeostasis by regulating the stability and function of sterol regulatory element-binding protein [SREBP] and SREBP cleavage-activating protein, J. Biol. Chem. 292 (7) (2017) 3016–3028.
[83] D. Eberle, B. Hegarty, P. Bossard, P. Ferre, F. Foufelle, SREBP transcription factors: master regulators of lipid homeostasis, Biochimie 86 (11) (2004) 839–848.
[84] D. Simar, A. Jacques, C. Caillaud, Heat shock proteins induction reduces stress kinases activation, potentially improving insulin signalling in monocytes from obese subjects, Cell Stress Chaperones 17 (5) (2012) 615–621.
[85] Y. Liu, A. Beyer, R. Aebersold, On the dependency of cellular protein levels on mRNA abundance, Cell 165 (3) (2016) 535–550.
[86] I.G. Cannell, Y.W. Kong, M. Bushell, How do microRNAs regulate gene expression? Biochem. Soc. Trans. 36 (6) (2008) 1224–1231.
[87] H. Yang, X.L. Xu, H.M. Ma, J. Jiang, Integrative analysis of transcriptomics and proteomics of skeletal muscles of the Chinese indigenous Shaziling pig compared with the Yorkshire breed, BMC Genet. 17 (1) (2016) 80.
[88] A.M. Timperio, A. D'Alessandro, L. Pariset, G.M. D'Amici, A. Valentini, L. Zolla, Comparative proteomics and transcriptomics analyses of livers from two different Bos taurus breeds: "Chianina and Holstein Friesian", J. Proteome 73 (2) (2009) 309–322.
[89] N.M. Page, D.J. Butlin, K. Lomthaisong, P.J. Lowry, The human apolipoprotein L gene cluster: identification, classification, and sites of distribution, Genomics 74 (1) (2001) 71–78.
[90] D.M. Bickhart, Y. Hou, S.G. Schroeder, C. Alkan, M.F. Cardone, L.K. Matukumalli, J. Song, R.D. Schnabel, M. Ventura, J.F. Taylor, J.F. Gacia, C.P. Van Tassel, Sonstergard. TS, E.E. Eichler, G.E. Liu, Copy number variation of individual cattle genomes using next-generation sequencing, Genome Res. 22 (4) (2012) 778–790.
[91] H. Zhang, Y. Wang, J. Li, J. Yu, J. Pu, L. Li, H. Zhang, S. Zhang, G. Peng, F. Yang, P. Liu, Proteome of skeletal muscle lipid droplet reveals association with mitochondria and apolipoprotein a-I, J. Proteome Res. 10 (10) (2011) 4757–4768.
[92] B. Ganss, A. Jheon, Zinc finger transcription factors in skeletal development, Crit. Rev. Oral Biol. Med. 15 (5) (2004) 282–297.
[93] W. Liu, D. Morito, S. Takashima, Y. Mineharu, H. Kobayashi, T. Hitomi, H. Hashikata, N. Matsuura, S. Yamazaki, A. Toyoda, K.-I. Kikuta, Y. Takagi, K.H. Harada, A. Fujiyama, R. Herzig, B. Krischek, L. Zou, J.E. Kim, M. Kitakaze, S. Miyamoto, K. Nagata, N. Hashimoto, A. Koizumi, Identification of RNF213 as susceptibility gene for moyamoya disease and its possible role in vascular development, Plos One 6 (7) (2011) e22542.
[94] B. Scholz, C. Korn, J. Wojtarowicz, C. Mogler, I. Augustin, M. Boutros, C. Niehrs, H.G. Augustin, Endothelial RSPO3 controls vascular stability and pruning through non-canonical WNT/Ca(2+)/NFAT signaling, Dev. Cell 36 (1) (2016) 79–93.
[95] C. Christodoulides, C. Lagathu, J.K. Sethi, A. Vidal-Puig, Adipogenesis and WNT signalling, Trends Endocrinol. Metab. 20 (1) (2009) 16–24.